Cell PRESS
Immunity
Article

pH-Dependent Interdomain Tethers of CD1b Regulate Its Antigen Capture

Miguel Relloso,[1] Tan-Yun Cheng,[1] Jin S. Im,[2] Emilio Parisini,[3] Carme Roura-Mir,[1] Charles DeBono,[1] Dirk M. Zajonc,[5,6] Leonel F. Murga,[4] Mary Jo Ondrechen,[4] Ian A. Wilson,[5] Steven A. Porcelli,[2] and D. Branch Moody[1,*]
[1]Division of Rheumatology, Immunology, and Allergy, Brigham and Women's Hospital and Harvard Medical School, Smith Building Room 514, 1 Jimmy Fund Way, Boston, MA 02115, USA
[2]Department of Microbiology and Immunology, Albert Einstein College of Medicine, Bronx, NY 10461, USA
[3]Laboratory of Immunobiology, Department of Medical Oncology, Dana-Farber Cancer Institute, Department of Medicine, Harvard Medical School, Boston, MA 02115, USA
[4]Department of Chemistry and Chemical Biology, Northeastern University, Boston, MA 02115, USA
[5]Skaggs Institute for Chemical Biology, The Scripps Research Institute, 10550 North Torrey Pines Road, La Jolla, CA 92037, USA
[6]Present address: Division of Cell Biology, La Jolla Institute for Allergy and Immunology, La Jolla, CA 92037, USA
*Correspondence: bmoody@rics.bwh.harvard.edu
DOI 10.1016/j.immuni.2008.04.017

SUMMARY

As CD1 proteins recycle between the cell surface and endosomes, they show altered receptiveness to lipid antigen loading. We hypothesized that changes in proton concentration encountered within distinct endosomal compartments influence the charge state of residues near the entrance to the CD1 groove and thereby control antigen loading. Molecular dynamic models identified flexible areas of the CD1b heavy chain in the superior and lateral walls of the A′ pocket. In these same areas, residues that carry charge in a pH-dependent manner (D60, E62) were found to tether the rigid α1 helix to flexible areas of the α2 helix and the 50-60 loop. After disruption of these tethers with acid pH or mutation, we observed increased association and dissociation of lipids with CD1b and preferential presentation of antigens with bulky lipid tails. We propose that ionic tethers act as molecular switches that respond to pH fluxes during endosomal recycling and regulate the conformation of the CD1 heavy chain to control the size and rate of antigens captured.

INTRODUCTION

CD1 proteins are antigen-presenting molecules that are encoded outside the MHC but share structural similarities with MHC class I and II molecules (Calabi and Milstein, 1986; Porcelli, 1995). Whereas MHC class I and class II molecules bind peptides, CD1 molecules use a hydrophobic cavity to capture lipid antigens for presentation to T cells (Zeng et al., 1997; Gadola et al., 2002; Zajonc et al., 2003) Antigens presented by the CD1 system are chemically diverse self- and foreign lipids, including mycolates, diacylglycerols, sphingolipids, polyisoprenols, polyketides, and lipopeptides (De Libero and Mori, 2005). Many studies show that subcellular microenvironments normally influence antigen-loading reactions in ways that allow cellular CD1 proteins to selectively capture specialized classes of lipid antigens from among the diverse pool of cellular lipids (Moody et al., 2005). In particular, CD1 proteins markedly alter their receptivity for loading lipid antigens as they move through secretory, cell-surface, and endosomal compartments prior to re-emerging on the cell surface to encounter T cell receptors (Sullivan et al., 2005).

During their rapid egress through the secretory pathway (Jayawardena-Wolf et al., 2001; Briken et al., 2002), CD1 proteins bind to abundant self-phospholipids, including phosphatidylinositol and phosphatidylcholine (Joyce et al., 1998; De Silva et al., 2002; Garcia-Alles et al., 2006), in a process that is regulated by microsomal trigyceride transport protein (Brozovic et al., 2004; Dougan et al., 2007). CD1 proteins subsequently reach endosomes either by being directly transited from the trans-golgi network (Kang and Cresswell, 2002) or by exiting to the surface and then being reinternalized into endosomes via a series of interactions known as the recycling pathway. Each CD1 isoform recycles through somewhat distinct subcompartments of the endosomal network on the basis of how differing cytoplasmic-tail sequences of each CD1 isoform interact with cytosolic adaptor protein complexes (AP-1, AP-2, AP-3) (Briken et al., 2000; Dascher and Brenner, 2003). As a result of their ability to bind to both AP-2 and AP-3 complexes, human CD1b and mouse CD1d proteins accumulate at particularly high levels in lysosomal compartments (Sugita et al., 1996; Briken et al., 2002; Sugita et al., 2002; Elewaut et al., 2003). After moving through the endosomal network, the recycling pathway involves transport of CD1 proteins back to the cell surface for presentation of lipids to T cells.

A general model emerging from these studies is that newly synthesized CD1 proteins first bind to endogenous chaperone lipids while transiting along the secretory pathway and then exchange these endogenously acquired lipids for exogenous antigens as they recycle through endosomes. Although there is currently no detailed molecular understanding of how such exchange reactions occur, this model derives considerable support from studies showing that the transport of CD1 proteins through late endosomal compartments influences the subsequent display of lipid antigens at the cell surface. For example, phagocytosis and receptor-mediated endocytosis by the macrophage mannose receptor (CD206), Langerin (CD207),

DC-SIGN (CD209), and low-density lipoprotein receptors (LDL-R) promote antigen display to T cells (Prigozy et al., 1997; Tailleux et al., 2003; Hunger et al., 2004; van den Elzen et al., 2005; Roura-Mir et al., 2005). In addition, even when large pools of CD1 proteins are present at the surface, recycling of CD1 proteins to late endosomes is required for antigen display. This conclusion derives from experiments showing that fixation of membranes, neutralization of pH, and deletion of interactions between the cytoplasmic tail and adaptor proteins block CD1b-mediated presentation of long-chain mycolic acid, lipoarabinomannan, C_{80} glucose monomycolate, and diacylated trehalose antigens to T cells (Porcelli et al., 1992; Sieling et al., 1995 Moody et al., 2002; Gilleron et al., 2004) . Furthermore, CD1d recycling is required for the activation of invariant NK T cells in vitro and in vivo (Chiu et al., 1999; Chiu et al., 2002; Roberts et al., 2002).

These studies clearly point to late endosomes and lysosomes as functionally important sites for the intersection of CD1 and lipid trafficking pathways and underscore the need to understand the role of endosomal factors in loading and unloading of antigens. Endosomes are enriched for lipid-binding proteins, including saposins, apolipoprotein E (apoE), and CD1e, which promote CD1-restricted T cell activation or positive selection (Kang and Cresswell, 2004; Winau et al., 2004; Zhou et al., 2004; de la Salle et al., 2005; van den Elzen et al., 2005). Also, endosomally localized glycosidases can act on glycolipids to expose epitopes of antigens that have been internalized into endosomes (Shamshiev et al., 2000; Zhou et al., 2004; de la Salle et al., 2005). In addition to the role of such extrinsic protein cofactors, antigen loading is regulated by the low pH (4.5–5.5) environment of late endosomes and lysosomes. Presentation of certain mycolate, diacylglycerol, and sphingolipid antigens requires a pH that is reduced to levels normally found in late endosomes (Porcelli et al., 1992; Sieling et al., 1995; Shamshiev et al., 2000; Moody et al., 2002; Gilleron et al., 2004; de la Salle et al., 2005). Simplified, cell-free experimental systems show that the acidic pH directly promotes binding of lipids to CD1 (Ernst et al., 1998; Gumperz et al., 2000) and presentation to T cells (Gumperz et al., 2000; Cheng et al., 2006). Thus, a central mechanism by which low pH promotes antigen display probably involves altering the conformation of CD1-β2 microglobulin complexes.

To evaluate the hypothesis that the structures of CD1 proteins are dynamically altered in response to acid pH, we focused on CD1 conserved structural elements located near the portal, which is the presumed site of antigen entry into the groove. After loading reactions are complete, lipid antigens are seated deeply within the α1-α2 superdomain in such a way that their hydrophilic head groups lie within the portal and the aliphatic hydrocarbon chains are sequestered within four hydrophobic pockets, known as A′, F′, C′, and T′ (Zeng et al., 1997; Gadola et al., 2002; Zajonc et al., 2003; Batuwangala et al., 2004; Koch et al., 2005; Zajonc et al., 2005; Garcia-Alles et al., 2006; Wu et al., 2006). A roof-like structure blocks direct entry into the top of the A′ pocket, and the portal is thus located off-center, over the F′ pocket in all CD1 proteins studied to date. Therefore, the F′ pocket is the likely site of antigen entry into the groove, and residues located within or near the portal and A′ roof regions probably interact with antigens during the loading process.

Several studies show that antigens with the largest alkyl chains have more stringent requirements for loading (Moody et al., 2002; Gilleron et al., 2004; Cheng et al., 2006). Therefore, we hypothesized that the narrow portal plays a role in regulating antigen exchange, such that large lipids encounter greater steric hindrance as they enter into the groove (Moody et al., 2005). Here we report that acidic pH disrupts ionic interactions involving two key amino acids (D60 and E62) that tether what would otherwise be structurally distinct domains near the CD1b portal. Disruption of these interdomain tethers strongly affected the size of antigens presented and the rate of antigen capture, leading to a detailed model explaining how pH fluctuations experienced by recycling CD1b proteins regulate antigen entry and exit from the groove.

RESULTS

Molecular-Dynamic Modeling of CD1b

In considering which parts of a CD1 protein might interact with antigens as they enter and exit the groove, we first compared the size and shape of the portals in MHC and CD1b antigen-presenting molecules. MHC class I and II grooves are open to solvent over most of their length, and antigens can directly enter the groove region with little steric interference from the residues that line the groove (Figure 1A, green). In contrast, the entrance to the groove of CD1b is partially blocked by the A′ roof, a structure formed by side chains positioned between the α1 and α2 helices and an interdomain ionic interaction formed by residue E62 located on α1 and basic resides (R168) on α2 (Figure 1A). Therefore, despite the fact that CD1b has a much larger internal cavity (2200 $Å^3$) than MHC class I molecules, crystal structures solved at neutral pH suggest that the portal for groove access is much narrower (15 Å versus ~25 Å) (Gadola et al., 2002; Batuwangala et al., 2004).

A second notable structural feature present in CD1b is a cluster of basic and acidic residues that form a network of charge-charge interactions involving the A′ roof and adjacent areas of the α1 and α2 helices (Figure 1A, red and blue). The actual charge state of acidic and basic amino acid side chains varies as a function of the pH to which the protein is exposed. The ratios of charged and uncharged forms of each of the side chains change according to the degree to which the local pH environment of the protein differs from the known pK_a of each side chain. These effects can be estimated according to the following formula, where A and B are acidic and basic ionizable residues, respectively:

$$pH - pK_a = \log_{10}([A-]/[AH]) = \log_{10}([B]/[HB+]). \quad (1)$$

Because the nominal pK_a values of lysine (~10.5) and arginine (~12.5) side chains are more than three units above the range of cellular pH, they normally remain positively charged during the entire range of pH encountered during endosomal recycling. In contrast, the nominal pK_a values of glutamate (4.1) and aspartate (3.9) side chains are near the pH range of late endosomes and lysosomes found in dendritic cells (4.5–5.5) (Trombetta et al., 2003). Accordingly, a fraction of the negatively charged side chains is predicted to accept a proton to become uncharged at pH levels found in lysosomes, but virtually all of these residues

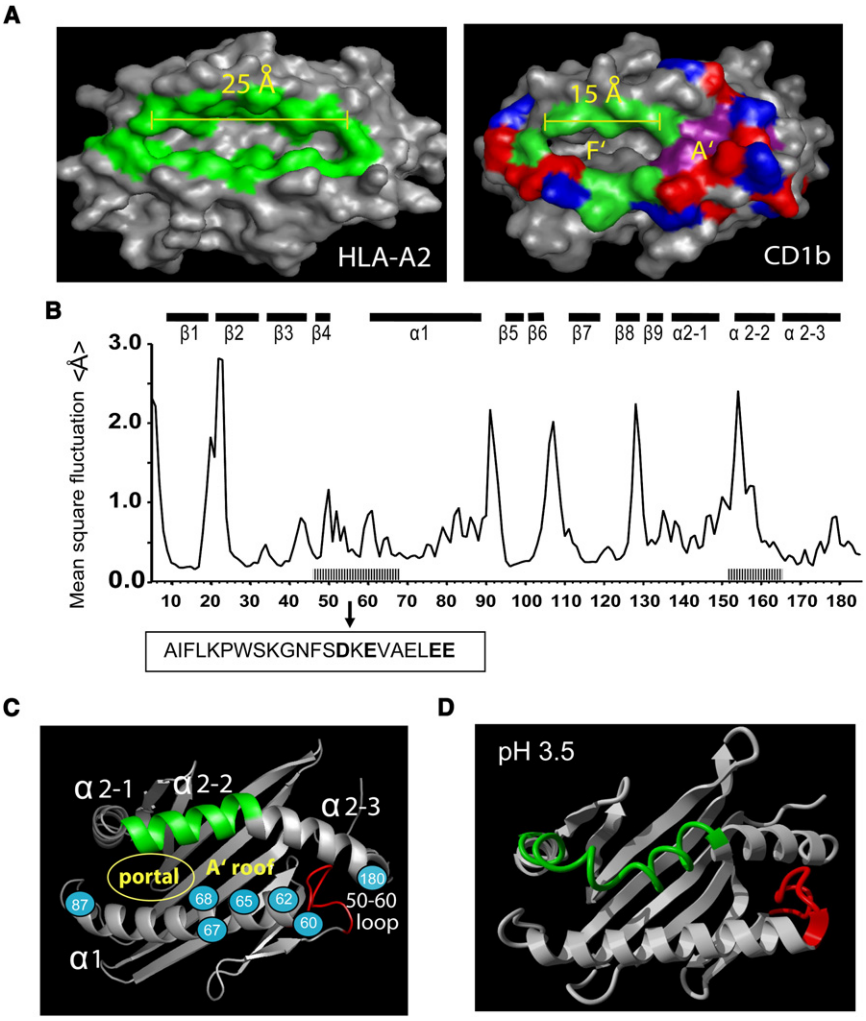

Figure 1. Molecular-Dynamics Modeling of CD1b

(A) Whereas residues that line the entrance (green) provide broad access to the HLA-A2 groove, the entrance to CD1b groove is located over the F' pocket and is narrowed by a roof-like structure (A' roof) formed by side chains positioned between the α1 and α2 helices (purple). Regions near the antigen portal contain many basic (blue) and acidic (red) amino acids that can be ionized to carry positive or negative charges.

(B) Molecular-dynamics modeling of the CD1b-β2 microglobulin complex (10,000 ns, pH 7.4, 300 K) is summarized with the computed mean-square fluctuations (MSFs) across the CD1b heavy chain, which is displayed on the X axis according to residue number and secondary structural elements: α1 helix (α1), α2 subhelices (α2-1, α2-2, α2-3), and β-strands (β1-6). The sequence of amino acids on the 50-60 loop is shown with bold letters indicating residues that were mutated.

(C) A ribbon diagram of CD1b at neutral pH showing residue numbers of anionic amino acids chosen for mutation (blue circles) and areas of high MSF, including the α2-2 subhelix (green) and the 50-60 loop (red).

(D) Representative still image of CD1b molecular-dynamics model carried out at pH 3.5 shows localized unraveling of the α2-2 helix to form a loop (green).

would be expected to carry a negative charge at the neutral pH found at the cell surface. Thus, the 100- to 1000-fold change in proton concentration normally experienced by CD1b proteins during endosomal recycling is predicted to reversibly alter the charge state of the glutamate and aspartate residues. Therefore, certain acidic residues near the portal (D60, E62, E65, E67, E68, E80, D83, D87, E156, E164, and D180) were considered good candidates for mediating pH-dependent changes in the CD1b structure.

Crystal structures show that the antigen-binding groove is formed by a β sheet floor supporting the α1 (positions 60–87) and α2 helices (positions 151–182). The α1 helix is a single, tight coil, whereas the helical structure of the α2 domain is intermittently interrupted so that it contains three subhelices, α2-1, α2-2, and α2-3. To predict pH effects on CD1b structure, we performed molecular-dynamics simulations with previously solved CD1b crystal structures (Gadola et al., 2002; Garcia-Alles et al., 2006). Molecular-dynamics simulations start with the three-dimensional structure of the protein and solve Newton's equations of motion for the atoms in that structure based on an empirical force field that describes the forces of attraction and repulsion between the atoms of the protein and between these atoms and the solvent molecules (Rapaport, 2004). Such simulations have been tested and used extensively for modeling the thermal motion of proteins and also enable studies of protein motion as a function of temperature and pH (Bonifati et al., 2003; Krieger et al., 2004; Baaden and Sansom, 2004).

Dynamic simulations at pH 7.2 over 10,000 ps measured the predicted mean square fluctuation (MSF) of the CD1b heavy chain over its entire length. This simulation predicted only small conformational perturbations in the α helices and β strand-forming segments of the CD1b heavy chain (Figure 1B). As expected, high MSF values were seen for loops that connect strands within the floor of the groove (residues 17–24, 33–34, 44–45, 91–92, 106–110, 119–121, and 127–130). In addition, elevated MSF values were observed in the second subhelix of the α2 domain (residues 153–159) and in the large loop formed by residues 50–60 (50–60 loop), which connect the α1 helix to the β sheet floor (residues 49–54 and 58–61).

Two of these areas were considered to be potentially important for antigen loading. First, the 50–60 loop forms the lateral wall of the A′ pocket (Figure 1C, red). This loop is the only long stretch of CD1b sequence within the antigen-binding site that does not fold into more stable secondary structure elements such as helices or strands. Second, the α2-2 subhelix is located between the antigen portal and the A′ roof (Figure 1C, green) in such a way that any flexibility in this region might alter the configuration of the antigen portal. Among all regions of the α2 helix, the highest MSF values were predicted to occur in the α2-2

subhelix (Figures 1B and 1D and data not shown). No substantial changes in structure were predicted to occur in the larger, well-formed α1 helix. Furthermore, when we carried out molecular-dynamics modeling by simulating acidic pH (3.5), the α2-2 subhelix was predicted to unfold in such a way that it alternates between helical and loop conformations (Figure 1D). This result is in agreement with previous circular dichroism analysis, which likewise predicted loss of α-helical structure below pH 5 (Ernst et al., 1998). Thus, these simulations of protein dynamics identified two areas of possible structural flexibility on the top (α2-2 subhelix) and side (50–60 loop) of the A′ pocket. These areas overlap with the location of charged residues near the portal, providing a second rationale for using mutagenesis to test the possibility that anionic residues in these locations regulate pH-dependent structural changes (Figure 1C, blue circles).

Mutagenesis of Periportal Amino Acids

To test the role of anionic residues in antigen presentation, we took advantage of an extensively validated experimental system involving CD1b presentation of the bacterial glycolipids known as glucose monomycolates (GMM) (Moody et al., 1997). The conformation of a GMM antigen within the CD1b groove is known from a crystal structure (Batuwangala et al., 2004), and GMM antigens have been produced in many forms that vary in the length and fine structure of their lipid tails; these forms include those that T cells recognize by cellular mechanisms that do or do not require endosomal factors (Moody et al., 2002; Cheng et al., 2006). We prepared a series of human CD1b cDNAs with point mutations involving glutamate and aspartate residues located near the portal, A′ roof, or 50–60 loop (D60, E62, E65, E67, E68, and D180) (Figure 1C). Alanine-scanning mutagenesis (D60A, E62A, E65A, E67A, E68A, and D180A) removes the ability to carry negative charge and also changes the size of the side chain in ways that reduce steric hindrance. We created a second set of mutations by substituting aspartate with asparagine and glutamic acid with glutamine (D60N, E62Q, E67Q, E68Q, and D180N), which conserves the overall size of the side chain and some of its hydrogen-bonding capability while removing the ability to form ionic bonds with basic residues. After stable transfection in C1R B lymphoblastoma cells, clones expressing wild-type or mutant proteins were matched for equivalent levels of CD1b cell-surface expression based on flow-cytometry analyses conducted at the time of functional studies (Figure S1A available online).

To evaluate antigen presentation, we measured the CD1b- and GMM-mediated activation of the CD1b-restricted clone LDN5. Also, we generated J.RT-3 cells stably transfected with the TCR α and β chains from LDN5, which allowed screening of a large number of mutant CD1b proteins. Initially, we screened mutants by using IL-2 release assays in which the form of GMM with long alkyl chains (C_{80} GMM) was added to CD1b-expressing cells. We carried out assays over 20 hr to allow extensive trafficking and endosomal transport of antigens for optimal loading. The effects of altering ionic interactions involving acidic amino acids on the top (E62 and E68) or side (D60, E67Q, and D180) of the A′ pocket or near the portal (D87) are summarized in Figure 2 and Figure S1B.

The CD1b mutant E67Q showed no effect on antigen presentation, and E68Q, D87N, and D180N showed 80%–90% percent decreases in the efficiency of glycolipid antigen presentation. Such loss-of-function mutations might have exerted their affects by controlling antigen loading or the shape of the CD1b-antigen complex with the TCR. More notable was the observation that CD1b mutants with absent or altered side chains at positions 60 and 62 presented C_{80} GMM to T cells 5- to 10-fold more efficiently than wild-type CD1b (Figure 2B and data not shown). This result was considered to be potentially important because it was unlikely that such a mutagenesis approach would fortuitously increase interactions with the TCR, and it was more likely to be influencing antigen loading. Also, gain-of-function mutations, as contrasted with loss-of-function mutations, are rare and are more likely to recapitulate a natural function of a protein.

In considering what features distinguish the two gain-of-function mutations from the many other mutations that do not promote function, we noted that the negatively charged acidic residues at positions 60 and 62 perform an interdomain tethering function and that the other tested residues do not have this function. Specifically, the side chain of E62 forms hydrogen bonds with R168 and K155 and an electrostatic interaction with R168, which is located near the second and third subhelices of α2 (Figure 2C). Thus, this mutation affects a residue that tethers the α1 helix to a potentially flexible region of the CD1b. Also, the E62-R168-K155 interaction forms a key part of the A′ roof. D60 forms an ionic bond with K55 located on the 50–60 loop and therefore tethers a central portion of a flexible loop to the distal, N-terminal end of the rigid α1 helix (Figure 2C, orange).

Thus, both gain-of-function mutations represented the loss of a negatively charged member of an ionic binding pair, and both of these pairs are involved in interdomain ionic interactions that tether the α1 helix to distant but flexible structural domains of CD1b. The gain of function might be explained if disruption of the ionic interaction resulted in partial or complete loss of these two tethering interactions that help to enclose the superior (E62) and lateral (D60) walls of the A′ pocket. These effects might increase the flexibility or volume of the A′ pocket in ways that facilitate the lipid entry, exit, or folding of the long meromycolate branch of the mycolic acid moiety, which makes a sharp turn near the wall formed by the 50–60 loop (Figure 1C, blue). Therefore, we studied these mutants in detail in various assays of lipid binding and antigen presentation.

CD1b Protein Binding to Lipids

To more directly measure the influence of mutations at positions 60 and 62 on lipid binding, we generated a set of recombinant proteins that comprised the extracellular domain of CD1b and were also altered at either proposed tethering site (D60A, E62A). We tested these hexahistidine-tagged single-chain CD1b-β2M proteins for their interactions with the fluorescent probe C6-HPC 2-(6-(7-nitrobenz-2-oxa-1,3-diazol-4-yl)amino)-hexanoyl-1-hexadecanoyl-*sn*-glycero-3-phosphocholine (NBD). This fluorescent probe has been used for directly measuring binding to CD1b and CD1c in aqueous buffers, and it mimics the dual alkyl chain with an approximate length of C_{25} lipids (Im et al., 2004). Preliminary experiments demonstrated no detectable changes in fluorescence when the probe was incubated with bovine serum albumin or fibronectin, which are used as

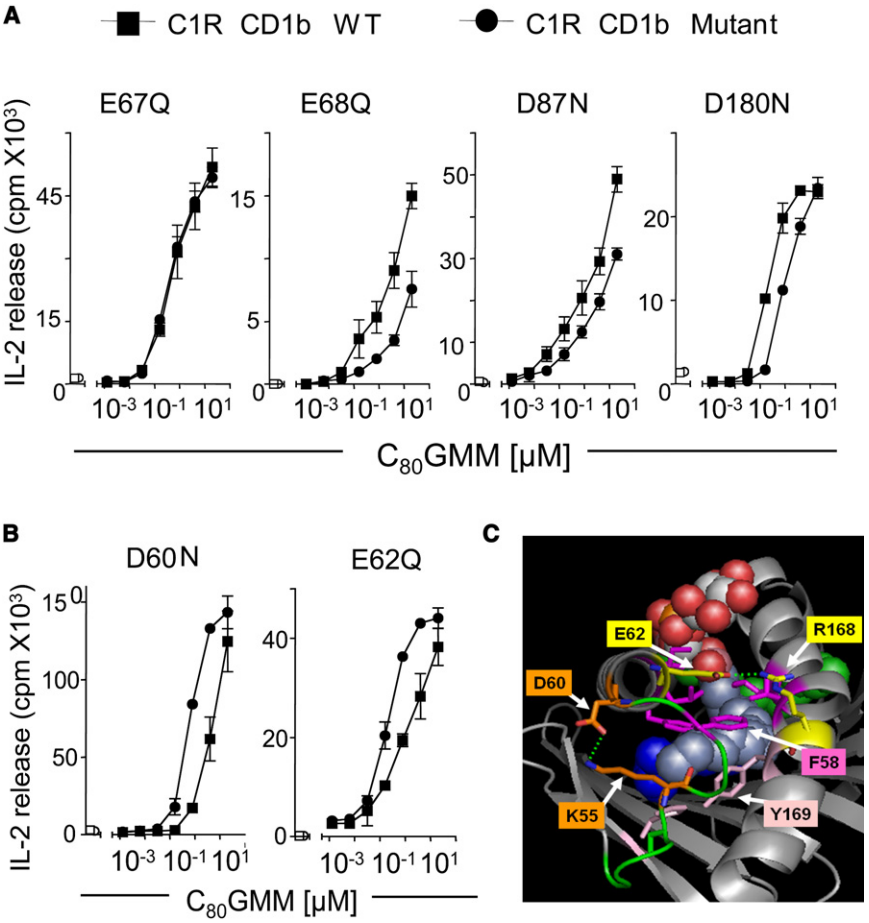

Figure 2. Screening CD1b Point Mutants to Identify Effects on Steady-State CD1b Antigen Presentation

(A and B) C1R B cell clones expressing wild-type (wt) CD1b or point mutants at equivalent levels were incubated with C_{80} GMM antigen and the CD1b-restricted T cell line LND5. After 20 hr, supernatants were tested for IL-2 production. In this and all figures, data are mean ± standard deviation of triplicate samples, and the results are representative of at least three experiments.

(C) Side view of the crystal structure of CD1b bound to glucose monomycolate (Gadola et al., 2002) shows that the location of the two amino acids whose deletion increased antigen presenting efficiency. The E62-R168 tether (yellow) connects the α1 helix across to the α2 helix, forming part of the A' roof (magenta). The D60-K55 interaction (orange) connects the α1 helix to the 50-60 loop (green), which together with two aromatic residues, F58 and Y169 (pink), forms the side wall of the A' pocket. The hydroxyl moieties on the mycolate and glucose ring (red) lie within and just outside the portal area. The proximal portion of the meromycolate lipid undergoes a nearly 360° turn within the A' pocket (light blue) and extends into the T' tunnel (dark blue).

controls for proteins that lack a hydrophobic groove. However, fluorescence was detected (Figure 3A) in a dose-dependent fashion (data not shown) when CD1b was added. Similar to results from prior studies using this (Im et al., 2004) and other hydrophobic probes (Ernst et al., 1998), we found that low pH (4.0) increased the measured fluorescence with NBD when incubated with CD1b (Figure 3A). Because the fluorescent properties of the probe were unaltered by changes in pH or the addition of proteins lacking hydrophobic grooves, these results were consistent with increased groove access induced by low pH.

Comparison of probe binding to mutant proteins at neutral and acidic pH showed that mutant proteins gave greater change in fluorescence than wild-type proteins in all cases (Figure 3B). Similar to results seen with wild-type proteins, the mutant proteins also showed increased fluorescence changes in response to low pH. The simultaneous application of low pH and tether deletion produced the greatest percentage change in fluorescence, but the combined effect of simultaneously applying both variables was less than the sum of the effects of applying each variable separately (Figure 3B). Collectively, these results indicate that both low pH and tether deletion promote access to the groove. Furthermore, the less than fully additive effects from simultaneous application of low pH and tether mutation are consistent with the interpretation that pH and deletion of tethering amino acids work by a shared mechanism.

Influence of Tether Mutation on Antigen Presentation at the Cell Surface

The IL-2 assays used to initially screen the panel of mutants required a 20 hr incubation, which allows extensive time for antigen uptake and transport throughout the cell. Therefore, this type of screening assay conducted under steady-state conditions measured the summed effect of mutations on loading reactions that occur in many subcellular compartments, including the cell surface and lysosomes. Prior studies have shown that the size of the lipid moiety and pH of the loading compartment strongly influence the outcomes of loading reactions (Moody et al., 2002; Cheng et al., 2006) . To more clearly isolate the effects of tethers and low pH, we carried out experiments under conditions that specifically measure processing at the cell surface and under conditions that mimic late endosomes.

First, we measured antigen-induced calcium flux occurring in T cells in response to antigen-presenting cells (APCs) pulsed with antigen for 15 min. This short time period is not sufficient for extensive CD1b recycling or antigen presentation after trafficking to endosomes, so this outcome selectively measures loading reactions that occur at or near the cell surface (Moody et al., 2002; Cheng et al., 2006). Also, if such assays are carried out in acidic media, the effects of higher proton concentrations that normally occur in late endosomes can be mimicked at the cell surface (Porcelli et al., 1992; Ernst et al., 1998; Moody et al., 2002). For wild-type CD1b, the antigen with short (C_{32} GMM) but not long alkyl chains (C_{80} GMM) was presented at neutral pH (Figure 4A). Lower pH promoted recognition of both antigens. The key difference was that presentation of C_{80} GMM was entirely dependent on acidification; a transition occurred in the range of pH 5.0–5.5.

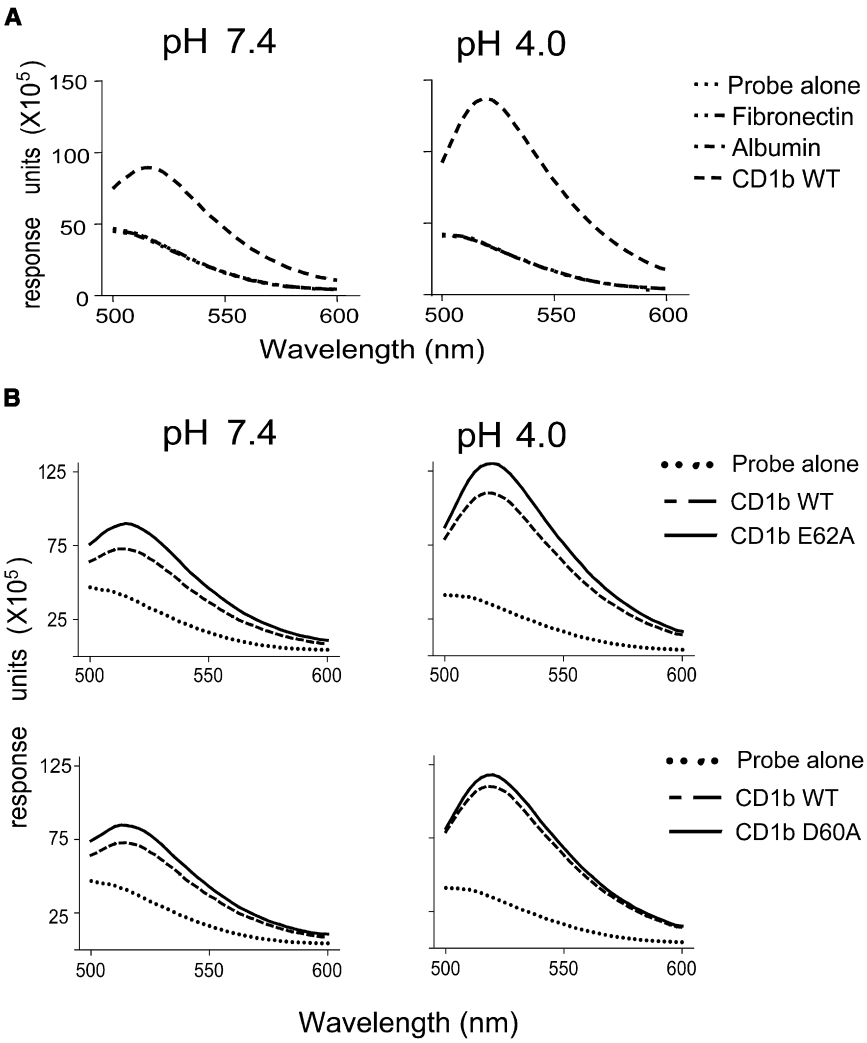

Figure 3. Acidic pH or Deletion of D60 or E62 Promote Lipid Binding to CD1b Proteins

(A) Recombinant hexahistidine-tagged CD1b, fibronectin, or bovine serum albumin was mixed with 2-fold molar excess of the fluorescent NBD-C6-HPC probe in citrate buffer at pH 7.4 or 4.0 and excited at 465 nm while the fluorescence emission spectra was read across the indicated wavelengths.

(B) Binding experiments with wild-type and mutant CD1b proteins were conducted as in (A) except that the reaction buffer was maintained for 1 hr at pH 7.4 or 4.0, and the NBD-C6-HPC probe was used at 10-fold molar excess. Results are representative of at least three experiments.

This system, in which the cellular location, chain-length dependence, and pH dependence of antigen-processing events are well defined, allowed testing of more detailed predictions of the postulated role of ionic tethers at positions 60 and 62. For C_{80} GMM, the D60N, D60A, and E62Q mutations markedly increased the efficiency of presentation, and the E62A mutation had a similar but less pronounced effect (Figure 4B, left panels). These results were similar to those seen in assays of binding (Figure 3) and steady-state presentation (Figure 2), confirming that mutations at positions 60 and 62 increase the efficiency of presentation of C_{80} GMM.

Notably, when an antigen with a shorter alkyl chain was used, each of the four point mutations provided the opposite effect and thus reduced the efficiency of C_{32} GMM presentation to T cells (Figure 4b, right). The net effect of each of the four point mutations in selectively promoting longer chain antigen recognition was strong, such that the relative efficiency of presentation of long- versus short-chain antigens, measured as the dose required for half-maximal T cell activation, increased by more than 10-fold after mutation. We then carried out similar experiments in the IL-2 steady-state screening assays and found that mutation at position 60 or 62 provided more augmentation to C_{80} (Figure 2A) than to C_{32} GMM (Figure S1C). Because mutation at either position 60 or 62 showed opposite effects on antigen presentation, depending on whether the short or long form of the antigen was used, these results suggest that a single tethering amino acid influences antigen selection on the basis of lipid length. Furthermore, because tether deletion favored presentation of antigens with long alkyl chains in all cases, this provided another reason to suggest that deletion of tethering amino acids increases groove access.

Influence of pH and Tether Mutation during Pulse-Chase

In considering possible mechanisms by which mutation could oppositely affect short- and long-chain antigens, we sought to carry out studies that separately measured loading and unloading events. Prior studies had suggested that long-chain antigens are more dependent on low pH for loading (Figure 4A and Porcelli et al., 1992; Shamshiev et al., 2002; Gilleron et al., 2004). Once loaded, long-chain lipids remain associated with CD1b-expressing cells for longer time periods than antigens with shorter alkyl chains (Moody et al., 2002). Tether loss might also affect unloading reactions and create a situation in which certain antigens are rapidly unloaded. Therefore, we developed an assay in which CD1b-expressing C1R clones were pulsed with antigen and then chased in antigen-free media (Figure 5A). Validation of this pulse-chase format with wild-type CD1b showed that loss of T cell activation during the chase period was more pronounced for C_{32} GMM than for C_{80} GMM in all cases, probably as a result of the smaller antigen's less extensive hydrophobic interactions with the groove. Also, washing antigen-pulsed cells in low pH media increased the loss of antigen-mediated T cell activation in all cases, as well as the degree of loss correlated with the extent of acidification (Figure 5A). Thus, low pH appears to promote antigen loss as well as antigen capture at steady state. Furthermore, in control experiments in which the protocol was modified so that acidic media was applied before rather than during the

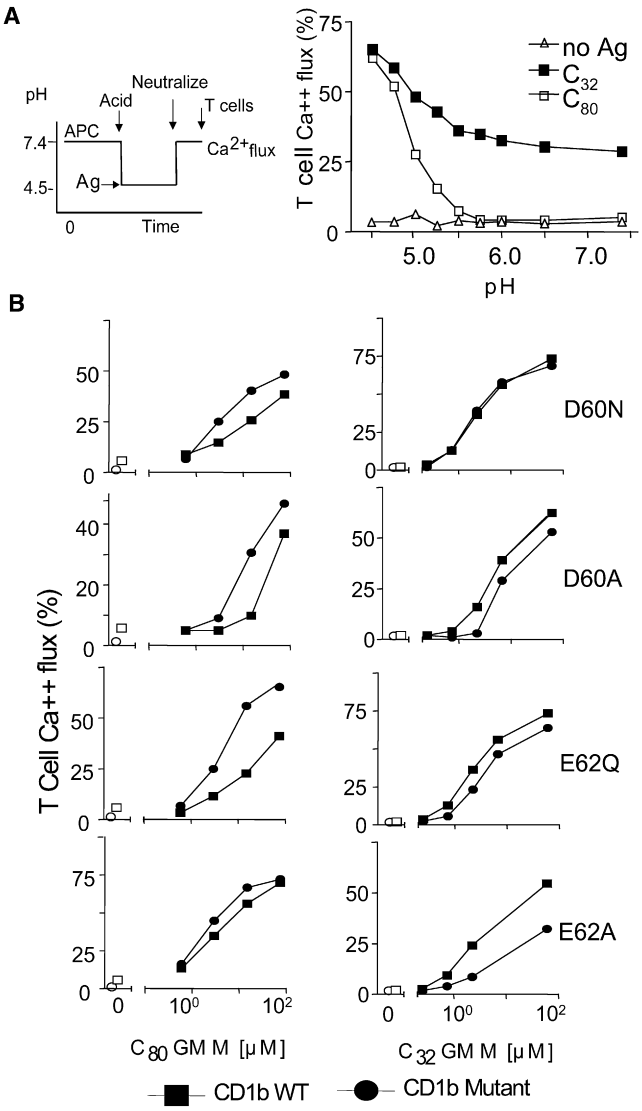

Figure 4. Pre-Steady-State Loading Assays Show that Low pH or Deletion of D60 or E62 Selectively Promotes Recognition of C_{80} GMM Antigens

(A) C1R cells expressing wild-type CD1b (APC) were cultured in media that was acidified to various levels between pH 4.5 and 7.4 after which short- (C_{32} GMM) or long-chain (C_{80} GMM) glucose monomycolate antigen was applied for 15 min prior to neutralizing the media and calcium flux was measured. (B) Via the method described in (A), C1R cells transfected with either wild-type CD1b proteins or point mutants expressing alanine, asparagine, or glutamine at the indicated position (D60N, D60A, E62Q, E62A) were tested for their ability to present C_{32} and C_{80} GMM to T cells. All results are representative of three or more experiments.

antigen pulse, no effects of pH on T cell activation were seen (Figure S2). The requirement that low pH be applied while antigens were in contact with CD1b indicated that the pH effect was fully reversible and therefore did not act by irreversible mechanisms such as the denaturation of CD1b or loss of β-2 microglobulin.

Acidification neutralizes the negative charges on aspartate and glutamate residues, including those that are predicted to form interdomain tethers, so the loss of T cell activation after acidification of media was consistent with an effect of tethers in promoting antigen retention. However, this effect may have been mediated through other effects on CD1 structure. To more specifically measure the effects mediated through positions 60 and 62, clones expressing mutant CD1b proteins were tested in the pulse-chase format. As with wild-type CD1b, T cell activation was more effectively retained in cells treated with C_{80} GMM than in those treated with C_{32} GMM, and low pH promoted loss of T cell stimulation (Figure 5B). Tether deletion increased loss of stimulation for both long- and short-chain antigens for each of the four single mutants. Next, we generated mutants with mutations in both tethers (D60A and E62A; D60N and E62Q) and found that doubly mutated proteins showed the greatest loss in stimulation during the chase period (Figure 5B).

To further test whether the small losses of antigenicity observed after 15 min were reproducibly controlled by tethering residues, we carried out a kinetic study of T cell activation over a time period of 120 min (Figure 5C). In all cases, tether mutation increased the rate of loss of antigen-dependent T cell stimulation. As seen previously in experiments carried out over a range of pH values, these kinetic measurements showed that the effects of both mutants altered at position 62, as compared to position 60, were stronger in absolute terms. The E62A and E62Q mutants, which have lost the tether located in the A′ roof, caused a decrease in the half-life of antigen-mediated T cell activation. Collectively, these data show that the removal of tether-forming amino acids or treatment reduces the duration of T cell activation by short- and long-chain antigens.

Residue-Specific Modeling and pKa Predictions

In agreement with binding studies (Ernst et al., 1998), data in Figure 4A suggest that the degree of acidification necessary to promote antigen display occurs at pH 5–5.5, which falls within the range of physiological pH of late endosomes. Using formula 1 and experimentally determined values of the pK_a of the side chains of aspartate and glutamate, one can estimate the percentage anionic residues that take on a charge at any given pH value. Whereas initial estimates of the charge states of glutamate and aspartate were obtained from the nominal pK_a values for the side chains of free amino acids and formula 1, the actual pK_a of individual ionizable side chains within folded protein is influenced, sometimes strongly, by nearby residues. Having identified D60 and E62 as the functionally important residues, we used the multiconformation continuum electrostatics (MCCE) method to model the charge state of these particular residues within the context of the known 3-dimensional structure of CD1b. This algorithm uses information from crystal structures to estimate the extent to which nearby amino acids in the folded protein influence ionizability of any given residue. Such calculated pK_a values have been shown to be more accurate than those derived from the free amino acid (Alexov and Gunner, 1997; Georgescu et al., 2002). By this method, theoretical titration curves for D60 and E62 in CD1b predict that nearly all side chains on D60 and E62 are negatively charged at neutral pH (Figure 6A). The pH range at which C_{80} GMM becomes presented (Figure 4A) correlates well with the pH range at which a substantial minority of the side chains at positions 60 and 62 are predicted to take on protons and lose their ability to form

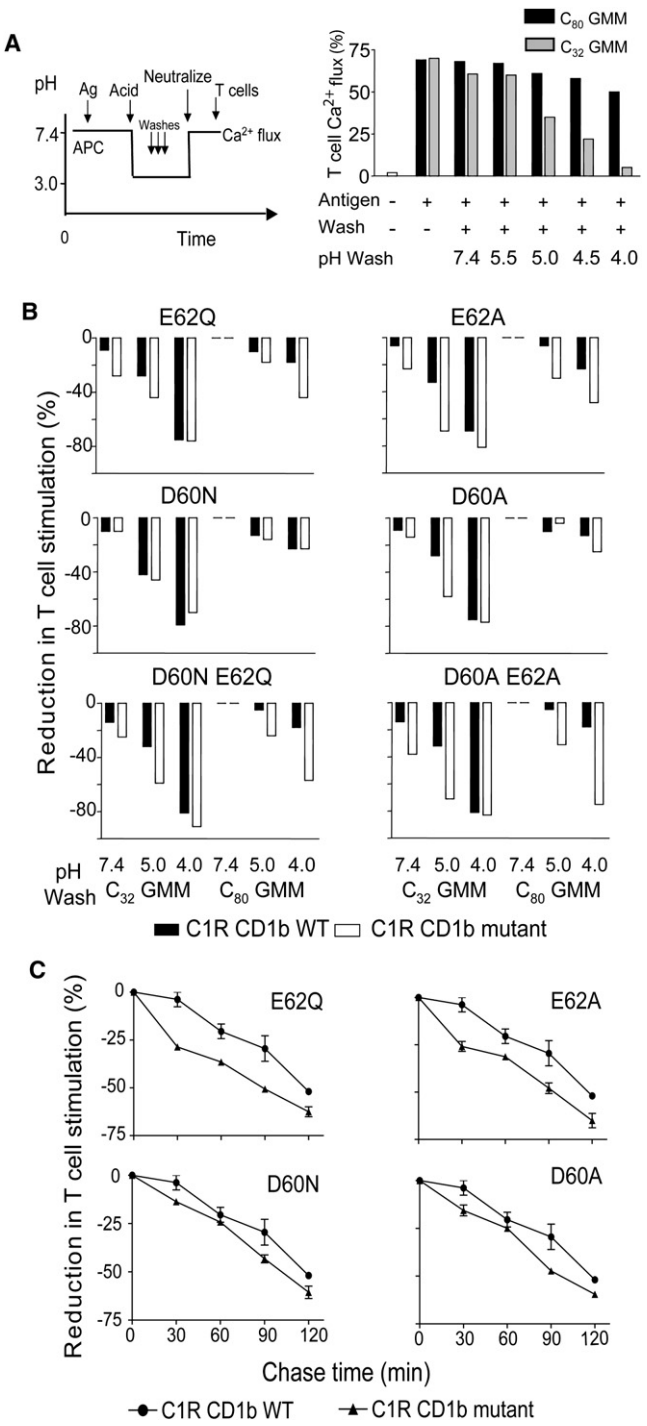

Figure 5. Pulse-Chase Assays Show that Low pH or Deletion of D60 or E62 Promotes Loss of T Cell Activation

(A) C1R cells expressing wild-type CD1b were treated with the antigen for 20 hr and then washed in antigen-free media at the designated pH prior to measuring T cell activation by calcium flux.

(B) C1R cells expressing CD1b proteins lacking one or both tethers as a result of single (D60N, D60A, E62Q, E62A) or double (D60N E62Q, D60A E62A) point mutations were analyzed as in (A).

(C) Kinetic experiments in which cells were washed and cultured for the indicated time were carried out at pH 5.0 with C_{80} GMM. The results are representative of at least three experiments.

salt bridges. Furthermore, MCCE calculations suggest that the pK_a of E62 is approximately one pH unit higher than that for D60, so this residue would be more extensively protonated and thus would be predicted to be more significantly influenced by the pH changes that result from recycling, as seen in assays of antigen presentation and unloading.

Finally, we used the three-dimensional models to estimate the relative solvent accessibility (RSA) of the amino acids involved in tethering and other types of ionic interactions. Electrostatic interactions are generally less stable for highly solvent exposed residues because Coulomb forces between charged residues are weaker in water, which has a high dielectric constant, than in a medium with low dielectric constant, such as the interior of a protein structure. The calculated RSA values for each of the mutated anionic amino acids in the periportal region show intermediate levels of accessibility (Figure 6B). D60 is the most solvent exposed of these residues. E62, the location that more strongly affects antigen presentation, is one of the least solvent exposed residues.

DISCUSSION

Although the dynamic process whereby lipids traverse the portal and first enter into CD1 grooves is poorly understood, crystal structures of CD1-lipid complexes provide detailed information relating to the final orientation of antigens within the α1-α2 superdomain after loading reactions are complete. If cellular CD1 proteins were strictly to adopt the conformations seen in the crystal structures, and if motion and mobility were not factors, antigens with long, folded alkyl chains would not gain access to the interior of the large A′ pockets at the earliest stages of insertion because the A′ roof would block access. Instead, they would in some way insert their acyl chains through the F′ portal, traverse the F′ pocket, and subsequently enter laterally into the broader A′ pocket. In the case of the unusually long meromycolate branch (C_{50-60}) of the C_{80} GMM antigen, this lipid must in some way be twisted into a tight, 360° loop within the A′ pocket. It is likely that the conformational changes that occur in CD1 heavy-chain folding before and during loading reactions influence the antigen exchange process. For example, a recent crystal structure of CD1d depicted one conformation bound to ligand and a second, markedly different conformation of CD1d with no well-defined density in the groove (Koch et al., 2005). The latter structure shows markedly altered periportal regions in which α1-α2 domain elements that normally encase lipids are flipped outward, increasing direct access to the groove. We now propose a detailed mechanism by which ionizable residues (D60 and E62) located near the portal act as pH-dependent molecular switches that control the rate and size selectivity of antigen binding and presentation by CD1b.

At neutral pH, E62 is fully ionized and forms an ionic bond with R168 to connect the α1 helix to the α2 helix in an interaction that blocks direct access into the A′ pocket at its superior margin. The α2-2 subhelix, which was found to be the most flexible periportal element in molecular-dynamics simulations, is located in the A′ roof, immediately adjacent to the portal and the E62-R168 tether. Therefore, both static and dynamic molecular modeling predict that loss of the E62-R168 tether would weaken the key interdomain interaction that closes the A′ roof.

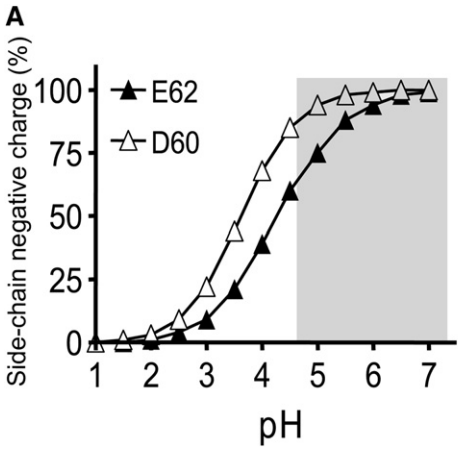

B

Residue	RSA (%)
D60	60.8
E62	22.6
E65	45.0
E67	15.4
E68	44.2
D180	31.6

Figure 6. Modeling the Influence of pH on CD1b Charge Based on Three-Dimensional Protein Structure

(A) With MCCE algorithms and crystal structure of CD1b, titration curves for residues E62 and D60 are expressed as the fraction of residues deprotonated in a large ensemble of protein molecules as a function of pH, compared to the range of pH encountered in endosomes (gray).

(B) Relative solvent accessibility (RSA) values for anionic amino acids subjected to point mutation. With Yasara software, the RSA is calculated as the ratio of solvent-exposed surface area of the indicated residue divided by the solvent-exposed surface area of residue X in the tripeptide GXG.

The intact D60-K55 interaction tethers the middle of the 50–60 loop and to the N-terminus of α1 helix. The 50–60 loop, including the bulky F58, forms the side wall of the A′ pocket. These structural considerations predict that disruption of the D60-K55 tether might allow the 50–60 loop to move laterally and thus increase the flexibility of the A′ pocket in ways that might facilitate the entry and twisting of alkyl chains so that they can take their final position in a looped conformation within the A′ pocket.

Increased proton concentrations encountered during endosomal recycling are predicted to partially neutralize the negative charges on D60 and E62 and lead to loss of the ionic components of the tethering interactions (Figure 6). The extent to which protonation of anionic amino acids leads to loss of tethering interactions depends on the Coulombic strength of the primary ionic interaction and the extent to which secondary hydrogen bonds compensate for the loss of the ionic interaction. Dynamic modeling exercises involving CD1b show how new secondary hydrogen-bonding interactions might form after the primary ionic bond is lost (data not shown). However, the experimental results show strong effects of mutation at positions 60 and 62, suggesting that such hydrogen-bonding interactions are not fully compensatory. Also, it is notable that substitution of these acidic side chains with either alanine or basic residues would be expected to have differing effects on hydrogen bonding. Alanine substitution largely removes hydrogen-bonding capacity, whereas asparagine and glutamine substitutions have side chains that might engage in hydrogen bonding. However, the two sets of mutants in which different amino acids are substituted at the same position have largely similar effects on antigen presentation. These results suggest that the ability to interact ionically with a positively charged binding partner, rather than hydrogen bonding, is the key variable in influencing function.

Point mutation and acidification are distinct experimental interventions that are both expected to disrupt tether function. Thus, acid pH and tether mutation are predicted to generate similar kinds of effects on binding and presentation when applied separately, and this was observed consistently. Whether simultaneous application of both interventions produces added effects depends on the extent to which mutation and acidification work via the same or separate mechanisms. If mutation removes all ionizable side chains or if acid protonates all side chains, then additive effects should not be seen. However, point mutation completely disrupts only one of many available tethers or ionizable interactions near the groove entrance. Acid pH acts on all ionizable residues in a protein, but it does so in a titratable fashion such that pH levels encountered in lysosomes are expected to neutralize only a minority of glutatmate and aspartate side chains. These considerations predict that simultaneous application of acid and mutation should produce effects that are stronger than each stimulus applied separately. However, the effect might be less than the sum of effects seen in response to each stimulus applied separately, a pattern that was observed consistently throughout these experiments.

One key aspect of these findings is that the effects of acid and mutation differ for presentation of short- and long-chain antigens. For wild-type CD1b, C_{32} GMM is readily loaded and unloaded, but C_{80} GMM has a greater barrier to being initially recognized and is lost much more slowly during chase in media, suggesting that the longer tails in C_{80} GMM impede both loading and unloading reactions. Thus, CD1b conformational changes that increase accessibility of the A′ pocket would be expected to selectively promote presentation of the long-chain antigens, and this effect is observed. Furthermore, even though many residues contribute to the shape of the interior surface of the groove, it is notable that the net effect of a single residue at position 60 or 62 is strong, such that the balance was shifted 20- to 200-fold toward preferential presentation of C_{80} GMM.

We have studied CD1b, but all types of CD1 antigen-presenting molecules studied to date recycle to some extent and are, therefore, candidates for using anionic residues as molecular switches. Human CD1a is the least attractive candidate because it can promiscuously bind lipids at the cell surface and does not efficiently traffic to low-pH compartments (Manolova et al., 2006; Sugita et al., 1999). Mouse CD1d is perhaps the best candidate because it, like human CD1b, fails to bind certain antigens at the cell surface (Porcelli et al., 1992; Sieling et al., 1995; Chiu et al., 1999; Chiu et al., 2002; Moody et al., 2002; Roberts et al., 2002; Gilleron et al., 2004) but selectively captures lipids after encountering high proton concentrations that affect the charge state of ionizable residues (Jayawardena-Wolf et al., 2001; Sugita et al., 2002; Lawton et al., 2005). Also, comparison of crystal structures identifies interdomain ionic interactions, including a K55-E177 interaction in the A′ roof, in mouse CD1d (Zajonc et al., 2005).

As CD1b proteins move through secretory, cell-surface, and endosomal compartments, they are exposed to a wide variety of potential lipid ligands that vary in their overall chain length. An integrated model of ligand selection by CD1b in which newly translated CD1b proteins capture endogenous short-chain ($<C_{50}$) lipids found ubiquitously within the secretory pathway is emerging; such lipids include phosphatidylinositols and phosphatidylcholines (Joyce et al., 1998; De Silva et al., 2002; Garcia-Alles et al., 2006). In this model, anionic amino acids engaged in interdomain tethering represent pH-regulated molecular switches, which are released by protonation and allow CD1b to transiently assume a conformation that promotes antigen exchange (rapid on-rapid off) when localized in endosomes. Exogenous lipids are sequestered in endosomes during infection by pathogens or the uptake of exogenous lipids or lipoprotein particles by mannose receptors, CD206, CD207, and CD209 or the LDL receptor. In this view, CD1b is like a pH-regulated lipid clamp that circulates within the cell in the closed state and then transiently opens to selectively receive lipids that are delivered from outside the antigen-presenting cell.

EXPERIMENTAL PROCEDURES

Recombinant Proteins

Wild-type human full-length CD1b heavy chain was cloned from pALTER-Max (Melian et al., 2000) with the forward oligonucleotide (5′-GCT CTA GAG CGC CGC CAC CAT GCT GCT GCT GCC ATT TCA ACT GTT-3′) and reverse (5′-TCC CCC GGG GGC TCA TGG GAT ATT CTG ATA TGA CC-3′) into pCI-neo (Promega Madison) with the use of XbaI and XmaI restriction sites, and constructs were verified by sequencing. Point mutations in the CD1b cDNA were introduced with the GeneTailor Site-Directed Mutagenesis System according to the manufacturer's (Invitrogen Carlsbad, CA) instructions (Demarchi et al., 2003; Melancon et al., 2004) and verified by sequencing. Vectors carrying CD1b wild-type or mutants were transfected into C1R B lymphoblastoid cells by electroporation with a Bio-Rad Gene Pulser II System. Transfectants were selected with 1 mg/ml G418 (Bio-Rad, Hercules CA). Clones and subclones were selected via flow-cytometric sorting for cells expressing high levels of CD1b.

All cells transfected with CD1b wild-type and mutant proteins were evaluated for CD1b surface expression by flow cytometry (BD FACSort, BD PharMingen, San Diego, CA) with a mAb to CD1b (4A7, BCD1b3.1, BCD1b2 and BCD1b7) (Melian et al., 2000) and stained with the secondary reagent fluorescein-isothiocyanate-conjugated goat anti-mouse Ig $F(ab')_2$ (Biosource, Camarillo, CA) within 72 hr of the completion of functional assays. In addition, selected mutants were permeabilized with NP-40, stained with a mAb to CD1b, and analyzed by flow cytometry so that the quantity of total cellular CD1b protein in comparison to the cell surface pool could be measured.

For expression of soluble single-chain (ssc) CD1b proteins lacking transmembrane and cytoplasmic sequences (Im et al., 2004), wild-type and CD1b mutants (D60A, E62A and D60A/E62) were cloned in pCDNA ssc CD1b encoding a hexahistidine tag (Im et al., 2004) by PCR with forward (5′-GGT GGA TCC GGT TCT GGA GGT GGA GGT TCA GAA CAT GCC TTC CAG GGG CCG ACC TCC TTT C-3′) and reverse (5′-GCG GCC GCC CTA CTA ATG GTG ATG GTG ATG GTG GCC CCC AAT TGA GCC AAT GGA GGT GGG G-3′) primers. Fragments were inserted between the BamHI and NotI sites in pCDNA ssc wild-type CD1b and verified by sequencing. Protein production was carried out in the FreeStyle 293 expression system (Invitrogen) according to the manufacturer's instructions (Bradley et al., 2003; Stengaard-Pedersen et al., 2003; Ido et al., 2004). Culture supernatants were incubated overnight with Ni-NTA agarose (Quiagen, Valencia CA) at 4°C. Beads were collected by centrifugation, placed in a column, and then extensively washed with PBS by gravity. CD1b proteins were then eluted with PBS containing 200 mM imidazole. Fractions were collected, and protein purity was assessed by reducing polyacrylimide gel electrophoresis analysis. Protein concentration was determined by UV absorption at 280 nm and anti-CD1b ELISA (Im et al., 2004), and studies were carried out in parallel on four batches of wild-type CD1b, two batches of D60A, and two batches of E62A with similar results.

T Cell Lines

The CD1b-restricted human αβ T cell line LDN5 specifically recognizes glucose monomycolate antigens with short (C_{32} GMM, purified from *R. equi*) and long (C_{80} GMM, purified from *M. phlei*) alkyl chains (Moody et al., 1997). To immortalize this line for testing with many CD1b proteins, we stably expressed LDN5 TCR α and β chains in J.RT-3 cells. The TCR α chain was cloned from pREP7 LDN5 TCR^- (Grant et al., 1999) by PCR with forward (5′-GGA ATT CCG CCG CCA CCA TGG AAA CTC TCC TGG GAG TGT C-3′) and reverse (5′-AGT TTA GCG GCC GCA TTC TTA TCA GCT GGA CCA CAA CCG CAG CG-3′) into in pCI-puro (Scott et al., 2002) at EcoRI and NotI positions. The TCR β chain was cloned from pREP9 LDN5 TCR β (Grant et al., 1999) by PCR with the forward primer 5′-GCT CTA GAG CGC CGC CAC CAT GGG CTG CAG GCT GCT CTG CTG TG and the reverse primer TCC CCC GGG GGA GCT AGC CTC TGG AAT CCT TTC TC-3′, and we inserted the PCR fragment in pCI-neo (Promega Madison WI) in XbaI/SmaI positions. Both plasmids were transfected the J.RT-3 cells (ATCC, Manassas, VA) by electroporation and selected with puromycin (0.6 μg/ml) and G418 (1 mg/ml), and the resulting cells were stained for CD3 (OKT3) expression and sorted by flow cytometry. J.RT-3/LDN5αβ stable transfectants and LND5 T cells both have the same antigen specificity, sensitivity, and CD1 restriction as seen in the native T cell lines.

T Cell Activation Assays

Steady State

Antigen presentation was measured by IL-2 release over 24 hr. Organic solvent was removed from stored antigens by drying under nitrogen, and this was followed by the addition of T cell media and sonication in a water bath for 2 min. For measuring T cell proliferation, 5×10^4 irradiated (7500 rad) C1R cells were incubated with antigen, and 5×10^4 LDN5 T cells or 1×10^5 JRT-3/LDN5 α/β cells were incubated with 10 ng/ml of phrobol myristate acetate (PMA) before supernatant was transfered to wells containing 5×10^3 IL-2-dependent HT-2 cells and [3H] thymidine was measured as described (Moody et al., 2002).

Cell-Surface-Presentation Assays

T cell calcium flux was measured after APCs were treated with antigen for 15 min. APCs (2×10^6 cells/ml) and antigens at 2× concentration were mixed 1:1 in Hank's Buffered Salt Solution with 1% bovine serum albumin (BSA) at the designated pH, which was adjusted by the addition of predetermined amounts of NaOH or HCl and confirmed with a pH meter. After 15 min, media were neutralized to 7.4 with an equal volume of buffered medium before the addition of T cells (10^6/ml) that had been preincubated with 4 μM Fura red and 2 μM Fluo-4 (Molecular Probes, Eugene, OR). APC and T cells were then added in equal volumes, subjected to centrifugation in a table-top centrifuge for 60 s, vortexed, and analyzed by flow cytometry as described (Moody et al., 2002).

Pulse-Chase Antigen-Presentation Assays

To measure loss of antigenic complexes, we treated 5×10^6 CD1b-expressing cells with antigens overnight at antigen doses previously determined to give half-maximal T cell activation and then washed three times with HBSS at the designated pH (4.0–7.4), resuspended at 1×10^6 cells/ml, added to an equal number of T cells, and subjected to calcium-flux measurements. For kinetic experiments, cells were washed three times at the outset and once prior to each time-dependent measurement. For control experiments to measure reversibility of the pH effect, cells were washed three times with HBSS at the designated pH (4.0–7.4), resuspended at 10^6 per ml for 30 min, neutralized to pH 7.4, and then treated with C_{32} GMM for 15 min before the addition of an equal number of T cells and the measurement of calcium flux.

CD1 Modeling

Molecular-dynamics simulations were performed with the Yasara suite of programs (Krieger et al., 2002; Krieger et al., 2004). Atomic coordinates were taken from the crystal structure (Gadola et al., 2002) with Protein Data Bank code 1GZQ. All ligands were removed. Glycosylation at N57, a post-translational modification that occurs in human cells but not in all protein expression systems, was built into the structure by use of the GLYCAM server. We generated parameters for the glycosylated Asn by using the Yasara AutoSMILE protocol to calculate the AM1-BCC (Jakalian et al., 2002; Wang et al., 2004)

charges and geometrical parameters for groups, such as modified amino acids, that are not included in standard force-field definitions. Hydrogen atoms were placed into the structure according to the computed pK_a for each residue at the pH of the simulation; an H^+ was placed at each ionizable position if the computed pK_a of that group was higher than the pH. For molecular-dynamics simulations, the pK_a values of the residues were computed within Yasara by an Ewald method (Krieger et al., 2006). The pH value of 3.0 was chosen as the basis for modeling the effects of low pH because it corresponded to a state in which E62 and D60 were both partially protonated and was within experimental values for which CD1b has been tested for binding β-2 microglobulin (Ernst et al., 1998). After placement of the hydrogen atoms, the structures were minimized by a steepest-descent method, followed by simulated annealing. Molecular-dynamics simulations were performed for 10 ns, and a temperature of 300K was assumed. Multiple time steps of 1 fs for intramolecular forces and 2 fs for intermolecular forces were used. Snapshots were saved every 500 fs for later analysis. The electrostatic potential and the theoretical titration curves were calculated with the multi-conformer continuum electrostatics (MCCE) method (Alexov and Gunner, 1997; Georgescu et al., 2002). Relative solvent accessibility (RSA) values were computed with Yasara.

Binding Assays

Binding assays were performed based on a modification of a prior method (Im et al., 2004) and were carried out at room temperature in saline buffer to pH in a range of 7.4–4.0 in a 1 cm × 0.2 cm quartz cuvette by means of a luminescence spectrometer (L550B, PerkinElmer) and the fluorescent probe 2-(6-(7-nitrobenz-2-oxa-1, 3-diazol-4-yl) amino) hexanoyl-1-hexadecanoyl-*sn*-glycero-3-phosphocholine (NBD C6-HPC) (Molecular Probes, Eugene, OR). The excitation wavelength for the solution was 465 nm, and the emission spectra were scanned from 490 to 600 nm. The protein (0.1 μM) and probe (1 μM) were mixed in citrate buffer at pH 7.4 or 4.0 for 1 hr prior the measurement of the fluorescence emission spectra.

SUPPLEMENTAL DATA

Two figures are available at http://www.immunity.com/cgi/content/full/28/6/774/DC1/.

ACKNOWLEDGMENTS

We are grateful to Rebeca Monje for her technical support. This work was supported by Pew Foundation Scholars in the Biomedical Sciences Program, the Burroughs Wellcome Fund, the Cancer Research Institute, the Mizutani Foundation for Glycoscience, the National Science Foundation (MCB-0517292), and the National Institutes of Health (AI 071155, AR048632, AI45889 and AI063537, CA58896 and GM62116).

Received: October 25, 2007
Revised: March 10, 2008
Accepted: April 15, 2008
Published online: June 5, 2008

REFERENCES

Alexov, E.G., and Gunner, M.R. (1997). Incorporating protein conformational flexibility into the calculation of pH-dependent protein properties. Biophys. J. *72*, 2075–2093.

Baaden, M., and Sansom, M.S. (2004). OmpT: Molecular dynamics simulations of an outer membrane enzyme. Biophys. J. *87*, 2942–2953.

Batuwangala, T., Shepherd, D., Gadola, S.D., Gibson, K.J., Zaccai, N.R., Fersht, A.R., Besra, G.S., Cerundolo, V., and Jones, E.Y. (2004). The crystal structure of human CD1b with a bound bacterial glycolipid. J. Immunol. *172*, 2382–2388.

Bonifati, V., Rizzu, P., van Baren, M.J., Schaap, O., Breedveld, G.J., Krieger, E., Dekker, M.C., Squitieri, F., Ibanez, P., Joosse, M., et al. (2003). Mutations in the DJ-1 gene associated with autosomal recessive early-onset parkinsonism. Science *299*, 256–259.

Bradley, K.A., Mogridge, J., Jonah, G., Rainey, A., Batty, S., and Young, J.A. (2003). Binding of anthrax toxin to its receptor is similar to alpha integrin-ligand interactions. J. Biol. Chem. *278*, 49342–49347.

Briken, V., Jackman, R.M., Dasgupta, S., Hoening, S., and Porcelli, S.A. (2002). Intracellular trafficking pathway of newly synthesized CD1b molecules. EMBO J. *21*, 825–834.

Briken, V., Moody, D.B., and Porcelli, S.A. (2000). Diversification of CD1 proteins: Sampling the lipid content of different cellular compartments. Semin. Immunol. *12*, 517–525.

Brozovic, S., Nagaishi, T., Yoshida, M., Betz, S., Salas, A., Chen, D., Kaser, A., Glickman, J., Kuo, T., Little, A., et al. (2004). CD1d function is regulated by microsomal triglyceride transfer protein. Nat. Med. *10*, 535–539.

Calabi, F., and Milstein, C. (1986). A novel family of human major histocompatibility complex-related genes not mapping to chromosome 6. Nature *323*, 540–543.

Cheng, T.Y., Relloso, M., Van Rhijn, I., Young, D.C., Besra, G.S., Briken, V., Zajonc, D.M., Wilson, I.A., Porcelli, S., and Moody, D.B. (2006). Role of lipid trimming and CD1 groove size in cellular antigen presentation. EMBO J. *25*, 2989–2999.

Chiu, Y.H., Jayawardena, J., Weiss, A., Lee, D., Park, S.H., Dautry-Varsat, A., and Bendelac, A. (1999). Distinct subsets of CD1d-restricted T cells recognize self-antigens loaded in different cellular compartments. J. Exp. Med. *189*, 103–110.

Chiu, Y.H., Park, S.H., Benlagha, K., Forestier, C., Jayawardena-Wolf, J., Savage, P.B., Teyton, L., and Bendelac, A. (2002). Multiple defects in antigen presentation and T cell development by mice expressing cytoplasmic tail-truncated CD1d. Nat. Immunol. *3*, 55–60.

Dascher, C.C., and Brenner, M.B. (2003). CD1 antigen presentation and infectious disease. Contrib. Microbiol. *10*, 164–182.

de la Salle, H., Mariotti, S., Angenieux, C., Gilleron, M., Garcia-Alles, L.F., Malm, D., Berg, T., Paoletti, S., Maitre, B., Mourey, L., et al. (2005). Assistance of microbial glycolipid antigen processing by CD1e. Science *310*, 1321–1324.

De Libero, G., and Mori, L. (2005). Recognition of lipid antigens by T cells. Nat. Rev. Immunol. *5*, 485–496.

De Silva, A.D., Park, J.J., Matsuki, N., Stanic, A.K., Brutkiewicz, R.R., Medof, M.E., and Joyce, S. (2002). Lipid protein interactions: The assembly of CD1d1 with cellular phospholipids occurs in the endoplasmic reticulum. J. Immunol. *168*, 723–733.

Demarchi, F., Bertoli, C., Sandy, P., and Schneider, C. (2003). Glycogen synthase kinase-3 beta regulates NF-kappa B1/p105 stability. J. Biol. Chem. *278*, 39583–39590.

Dougan, S.K., Rava, P., Hussain, M.M., and Blumberg, R.S. (2007). MTP regulated by an alternate promoter is essential for NKT cell development. J. Exp. Med. *204*, 533–545.

Elewaut, D., Lawton, A.P., Nagarajan, N.A., Maverakis, E., Khurana, A., Honing, S., Benedict, C.A., Sercarz, E., Bakke, O., Kronenberg, M., and Prigozy, T.I. (2003). The adaptor protein AP-3 is required for CD1d-mediated antigen presentation of glycosphingolipids and development of Valpha14i NKT cells. J. Exp. Med. *198*, 1133–1146.

Ernst, W.A., Maher, J., Cho, S., Niazi, K.R., Chatterjee, D., Moody, D.B., Besra, G.S., Watanabe, Y., Jensen, P.E., Porcelli, S.A., et al. (1998). Molecular interaction of CD1b with lipoglycan antigens. Immunity *8*, 331–340.

Gadola, S.D., Zaccai, N.R., Harlos, K., Shepherd, D., Castro-Palomino, J.C., Ritter, G., Schmidt, R.R., Jones, E.Y., and Cerundolo, V. (2002). Structure of human CD1b with bound ligands at 2.3 A, a maze for alkyl chains. Nat. Immunol. *3*, 721–726.

Garcia-Alles, L.F., Versluis, K., Maveyraud, L., Vallina, A.T., Sansano, S., Bello, N.F., Gober, H.J., Guillet, V., de la Salle, H., Puzo, G., et al. (2006). Endogenous phosphatidylcholine and a long spacer ligand stabilize the lipid-binding groove of CD1b. EMBO J. *25*, 3684–3692.

Georgescu, R.E., Alexov, E.G., and Gunner, M.R. (2002). Combining conformational flexibility and continuum electrostatics for calculating pK(a)s in proteins. Biophys. J. *83*, 1731–1748.

Gilleron, M., Stenger, S., Mazorra, Z., Wittke, F., Mariotti, S., Bohmer, G., Prandi, J., Mori, L., Puzo, G., and De Libero, G. (2004). Diacylated sulfoglycolipids are novel mycobacterial antigens stimulating CD1-restricted T cells during infection with Mycobacterium tuberculosis. J. Exp. Med. *199*, 649–659.

Grant, E.P., Degano, M., Rosat, J.P., Stenger, S., Modlin, R.L., Wilson, I.A., Porcelli, S.A., and Brenner, M.B. (1999). Molecular recognition of lipid antigens by T cell receptors. J. Exp. Med. *189*, 195–205.

Gumperz, J.E., Roy, C., Makowska, A., Lum, D., Sugita, M., Podrebarac, T., Koezuka, Y., Porcelli, S.A., Cardell, S., Brenner, M.B., and Behar, S.M. (2000). Murine CD1d-restricted T cell recognition of cellular lipids. Immunity *12*, 211–221.

Hunger, R.E., Sieling, P.A., Ochoa, M.T., Sugaya, M., Burdick, A.E., Rea, T.H., Brennan, P.J., Belisle, J.T., Blauvelt, A., Porcelli, S.A., and Modlin, R.L. (2004). Langerhans cells utilize CD1a and langerin to efficiently present nonpeptide antigens to T cells. J. Clin. Invest. *113*, 701–708.

Ido, H., Harada, K., Futaki, S., Hayashi, Y., Nishiuchi, R., Natsuka, Y., Li, S., Wada, Y., Combs, A.C., Ervasti, J.M., and Sekiguchi, K. (2004). Molecular dissection of the alpha-dystroglycan- and integrin-binding sites within the globular domain of human laminin-10. J. Biol. Chem. *279*, 10946–10954.

Im, J.S., Yu, K.O., Illarionov, P.A., LeClair, K.P., Storey, J.R., Kennedy, M.W., Besra, G.S., and Porcelli, S.A. (2004). Direct measurement of antigen binding properties of CD1 proteins using fluorescent lipid probes. J. Biol. Chem. *279*, 299–310.

Jakalian, A., Jack, D.B., and Bayly, C.I. (2002). Fast, efficient generation of high-quality atomic charges. AM1-BCC model: II. Parameterization and validation. J. Comput. Chem. *23*, 1623–1641.

Jayawardena-Wolf, J., Benlagha, K., Chiu, Y.H., Mehr, R., and Bendelac, A. (2001). CD1d endosomal trafficking is independently regulated by an intrinsic CD1d-encoded tyrosine motif and by the invariant chain. Immunity *15*, 897–908.

Joyce, S., Woods, A.S., Yewdell, J.W., Bennink, J.R., De Silva, A.D., Boesteanu, A., Balk, S.P., Cotter, R.J., and Brutkiewicz, R.R. (1998). Natural ligand of mouse CD1d1: Cellular glycosylphosphatidylinositol. Science *279*, 1541–1544.

Kang, S.J., and Cresswell, P. (2002). Calnexin, calreticulin, and ERp57 cooperate in disulfide bond formation in human CD1d heavy chain. J. Biol. Chem. *277*, 44838–44844.

Kang, S.J., and Cresswell, P. (2004). Saposins facilitate CD1d-restricted presentation of an exogenous lipid antigen to T cells. Nat. Immunol. *5*, 175–181.

Koch, M., Stronge, V.S., Shepherd, D., Gadola, S.D., Mathew, B., Ritter, G., Fersht, A.R., Besra, G.S., Schmidt, R.R., Jones, E.Y., and Cerundolo, V. (2005). The crystal structure of human CD1d with and without alpha-galactosylceramide. Nat. Immunol. *6*, 819–826.

Krieger, E., Darden, T., Nabuurs, S.B., Finkelstein, A., and Vriend, G. (2004). Making optimal use of empirical energy functions: Force-field parameterization in crystal space. Proteins *57*, 678–683.

Krieger, E., Koraimann, G., and Vriend, G. (2002). Increasing the precision of comparative models with YASARA NOVA–a self-parameterizing force field. Proteins *47*, 393–402.

Krieger, E., Nielsen, J.E., Spronk, C.A., and Vriend, G. (2006). Fast empirical pKa prediction by Ewald summation. J. Mol. Graph. Model. *25*, 481–486.

Lawton, A.P., Prigozy, T.I., Brossay, L., Pei, B., Khurana, A., Martin, D., Zhu, T., Spate, K., Ozga, M., Honing, S., et al. (2005). The mouse CD1d cytoplasmic tail mediates CD1d trafficking and antigen presentation by adaptor protein 3-dependent and -independent mechanisms. J. Immunol. *174*, 3179–3186.

Manolova, V., Kistowska, M., Paoletti, S., Baltariu, G.M., Bausinger, H., Hanau, D., Mori, L., and De Libero, G. (2006). Functional CD1a is stabilized by exogenous lipids. Eur. J. Immunol. *36*, 1083–1092.

Melancon, J.M., Foster, T.P., and Kousoulas, K.G. (2004). Genetic analysis of the herpes simplex virus type 1 UL20 protein domains involved in cytoplasmic virion envelopment and virus-induced cell fusion. J. Virol. *78*, 7329–7343.

Melian, A., Watts, G.F., Shamshiev, A., De Libero, G., Clatworthy, A., Vincent, M., Brenner, M.B., Behar, S., Niazi, K., Modlin, R.L., et al. (2000). Molecular recognition of human CD1b antigen complexes: Evidence for a common pattern of interaction with alpha beta TCRs. J. Immunol. *165*, 4494–4504.

Moody, D.B., Briken, V., Cheng, T.Y., Roura-Mir, C., Guy, M.R., Geho, D.H., Tykocinski, M.L., Besra, G.S., and Porcelli, S.A. (2002). Lipid length controls antigen entry into endosomal and nonendosomal pathways for CD1b presentation. Nat. Immunol. *3*, 435–442.

Moody, D.B., Reinhold, B.B., Guy, M.R., Beckman, E.M., Frederique, D.E., Furlong, S.T., Ye, S., Reinhold, V.N., Sieling, P.A., Modlin, R.L., et al. (1997). Structural requirements for glycolipid antigen recognition by CD1b-restricted T cells. Science *278*, 283–286.

Moody, D.B., Zajonc, D.M., and Wilson, I.A. (2005). Anatomy of CD1-lipid antigen complexes. Nat. Rev. Immunol. *5*, 387–399.

Porcelli, S., Morita, C.T., and Brenner, M.B. (1992). CD1b restricts the response of human CD4–8- T lymphocytes to a microbial antigen. Nature *360*, 593–597.

Porcelli, S.A. (1995). The CD1 family: A third lineage of antigen-presenting molecules. Adv. Immunol. *59*, 1–98.

Prigozy, T.I., Sieling, P.A., Clemens, D., Stewart, P.L., Behar, S.M., Porcelli, S.A., Brenner, M.B., Modlin, R.L., and Kronenberg, M. (1997). The mannose receptor delivers lipoglycan antigens to endosomes for presentation to T cells by CD1b molecules. Immunity *6*, 187–197.

Rapaport, D.C. (2004). The Art of Molecular Dynamics Simulations, Second Edition (Cambridge, UK: Cambridge University Press).

Roberts, T.J., Sriram, V., Spence, P.M., Gui, M., Hayakawa, K., Bacik, I., Bennink, J.R., Yewdell, J.W., and Brutkiewicz, R.R. (2002). Recycling CD1d1 molecules present endogenous antigens processed in an endocytic compartment to NKT cells. J. Immunol. *168*, 5409–5414.

Roura-Mir, C., Catalfamo, M., Cheng, T.Y., Marqusee, E., Besra, G.S., Jaraquemada, D., and Moody, D.B. (2005). CD1a and CD1c activate intrathyroidal T cells during Graves' disease and Hashimoto's thyroiditis. J. Immunol. *174*, 3773–3780.

Scott, S.D., Joiner, M.C., and Marples, B. (2002). Optimizing radiation-responsive gene promoters for radiogenetic cancer therapy. Gene Ther. *9*, 1396–1402.

Shamshiev, A., Donda, A., Prigozy, T.I., Mori, L., Chigorno, V., Benedict, C.A., Kappos, L., Sonnino, S., Kronenberg, M., and De Libero, G. (2000). The alpha-beta T cell response to self-glycolipids shows a novel mechanism of CD1b loading and a requirement for complex oligosaccharides. Immunity *13*, 255–264.

Shamshiev, A., Gober, H.J., Donda, A., Mazorra, Z., Mori, L., and De Libero, G. (2002). Presentation of the same glycolipid by different CD1 molecules. J. Exp. Med. *195*, 1013–1021.

Sieling, P.A., Chatterjee, D., Porcelli, S.A., Prigozy, T.I., Mazzaccaro, R.J., Soriano, T., Bloom, B.R., Brenner, M.B., Kronenberg, M., Brennan, P.J., et al. (1995). CD1-restricted T cell recognition of microbial lipoglycan antigens. Science *269*, 227–230.

Stengaard-Pedersen, K., Thiel, S., Gadjeva, M., Moller-Kristensen, M., Sorensen, R., Jensen, L.T., Sjoholm, A.G., Fugger, L., and Jensenius, J.C. (2003). Inherited deficiency of mannan-binding lectin-associated serine protease 2. N. Engl. J. Med. *349*, 554–560.

Sugita, M., Cao, X., Watts, G.F., Rogers, R.A., Bonifacino, J.S., and Brenner, M.B. (2002). Failure of trafficking and antigen presentation by CD1 in AP-3-deficient cells. Immunity *16*, 697–706.

Sugita, M., Jackman, R.M., van Donselaar, E., Behar, S.M., Rogers, R.A., Peters, P.J., Brenner, M.B., and Porcelli, S.A. (1996). Cytoplasmic tail-dependent localization of CD1b antigen-presenting molecules to MIICs. Science *273*, 349–352.

Sugita, M., Grant, E.P., van Donselaar, E., Hsu, V.W., Rogers, R.A., Peters, P.J., and Brenner, M.B. (1999). Separate pathways for antigen presentation by CD1 molecules. Immunity *11*, 743–752.

Sullivan, B.A., Nagarajan, N.A., and Kronenberg, M. (2005). CD1 and MHC II find different means to the same end. Trends Immunol. *26*, 282–288.

Tailleux, L., Schwartz, O., Herrmann, J.L., Pivert, E., Jackson, M., Amara, A., Legres, L., Dreher, D., Nicod, L.P., Gluckman, J.C., et al. (2003). DC-SIGN is

the major Mycobacterium tuberculosis receptor on human dendritic cells. J. Exp. Med. *197*, 121–127.

Trombetta, E.S., Ebersold, M., Garrett, W., Pypaert, M., and Mellman, I. (2003). Activation of lysosomal function during dendritic cell maturation. Science *299*, 1400–1403.

van den Elzen, P., Garg, S., Leon, L., Brigl, M., Leadbetter, E.A., Gumperz, J.E., Dascher, C.C., Cheng, T.Y., Sacks, F.M., Illarionov, P.A., et al. (2005). Apolipoprotein-mediated pathways of lipid antigen presentation. Nature *437*, 906–910.

Wang, J., Wolf, R.M., Caldwell, J.W., Kollman, P.A., and Case, D.A. (2004). Development and testing of a general amber force field. J. Comput. Chem. *25*, 1157–1174.

Winau, F., Schwierzeck, V., Hurwitz, R., Remmel, N., Sieling, P.A., Modlin, R.L., Porcelli, S.A., Brinkmann, V., Sugita, M., Sandhoff, K., et al. (2004). Saposin C is required for lipid presentation by human CD1b. Nat. Immunol. *5*, 169–174.

Wu, D., Zajonc, D.M., Fujio, M., Sullivan, B.A., Kinjo, Y., Kronenberg, M., Wilson, I.A., and Wong, C.H. (2006). Design of natural killer T cell activators: Structure and function of a microbial glycosphingolipid bound to mouse CD1d. Proc. Natl. Acad. Sci. USA *103*, 3972–3977.

Zajonc, D.M., Elsliger, M.A., Teyton, L., and Wilson, I.A. (2003). Crystal structure of CD1a in complex with a sulfatide self antigen at a resolution of 2.15 A. Nat. Immunol. *4*, 808–815.

Zajonc, D.M., Maricic, I., Wu, D., Halder, R., Roy, K., Wong, C.H., Kumar, V., and Wilson, I.A. (2005). Structural basis for CD1d presentation of a sulfatide derived from myelin and its implications for autoimmunity. J. Exp. Med. *202*, 1517–1526.

Zeng, Z., Castano, A.R., Segelke, B.W., Stura, E.A., Peterson, P.A., and Wilson, I.A. (1997). Crystal structure of mouse CD1: An MHC-like fold with a large hydrophobic binding groove. Science *277*, 339–345.

Zhou, D., Cantu, C., 3rd, Sagiv, Y., Schrantz, N., Kulkarni, A.B., Qi, X., Mahuran, D.J., Morales, C.R., Grabowski, G.A., Benlagha, K., et al. (2004). Editing of CD1d-bound lipid antigens by endosomal lipid transfer proteins. Science *303*, 523–527.